Modal and wavelength conversions in plasmonic nanowires

Adrian Agreda, Deepak Sharma, Gérard Colas Des Francs, G. Kumar, Alexandre Bouhelier

Research Article | Vol. 29, No. 10 / 10 May 2021 / Optics Express 15366
Optics EXPRESS

Modal and wavelength conversions in plasmonic nanowires

ADRIAN AGREDA,[1,2] DEEPAK K. SHARMA,[1,3] GÉRARD COLAS DES FRANCS,[1] G. V. PAVAN KUMAR,[3] AND ALEXANDRE BOUHELIER[1,*]

[1]Laboratoire Interdisciplinaire Carnot de Bourgogne, UMR 6303 CNRS, Université de Bourgogne Franche-Comté, 9 Avenue Alain Savary, 21000 Dijon, France
[2]LP2N, Institut d'Optique Graduate School, CNRS, Univ. Bordeaux, 33400 Talence, France
[3]Department of Physics, Indian Institute of Science Education and Research (IISER) Pune - 411008, India
*alexandre.bouhelier@u-bourgogne.fr

Abstract: We show that plasmonic nanowire-nanoparticle systems can perform nonlinear wavelength and modal conversions and potentially serve as building blocks for signal multiplexing and novel trafficking modalities. When a surface plasmon excited by a pulsed laser beam propagates in a nanowire, it generates a localized broadband nonlinear continuum at the nanowire surface as well as at active locations defined by sites where nanoparticles are absorbed (enhancement sites). The local response may couple to new sets of propagating modes enabling a complex routing of optical signals through modal and spectral conversions. Different aspects influencing the optical signal conversions are presented, including the parameters defining the local formation of the continuum and the subsequent modal routing in the nanowire.

1. Introduction

The realization of a functional and operational densely integrated nanophotonic circuitry largely depends on the development of the plasmonic components toolbox. Indeed, surface plasmon polaritons (SPPs) have the essential ability to concentrate light beyond the diffraction limit granting the possibility to manipulate light with very small device dimensions [1,2]. In this context, the deployment of plasmonic nanowires were highlighted because they enable a series of much needed functionalities such as transport, and routing [3], switching [4] as well as logic optical operations [5,6]. In particular, chemically synthesized silver nanowires (AgNWs) are of notable interest in this context [7,8]. Firstly because their crystalline structure, excellent diameter uniformity and surface smoothness mitigate SPP scattering losses allowing for longer surface plasmon propagation distances and a richer modal diversity [9]. Secondly, silver exhibits lower intrinsic losses than any other plasmonic material when operating in the visible spectral range [10]. Finally, these one-dimensional nanostructures can be easily and consistently prepared using solution-based processing methods [11,12].

The strong optical fields associated with the propagation of a SPP in a nanowire lead to enhanced light matter interactions, enabling under certain excitation conditions, the observation of nonlinear responses. These nonlinear effects are certainly widening the gamut of applications and functionalities that can be performed by systems with reduced dimensions [3,13]. In this context, engineering the plasmonic modal landscape is of great importance in the control of the nonlinear responses and the realization of complex optical transport and advanced information processing operations [14–16]. Particularly interesting is the switching of the transported energy between the different modes sustained by the waveguide. In nanowires, such modal conversion is typically achieved by introducing local symmetry-breaking sites [17]. In this work, we extend this concept to control a secondary modal distribution introduced by the material's nonlinear response. We specifically discuss a novel routing modality by introducing plasmonic-enabled

#421183 https://doi.org/10.1364/OE.421183
Journal © 2021 Received 29 Jan 2021; revised 19 Mar 2021; accepted 19 Mar 2021; published 4 May 2021

Optics EXPRESS

wavelength and mode conversion mechanisms based upon the nonlinear interaction between the SPP and nanoparticles adsorbed on the nanowire surface. We confirm the field-enhancing role of adsorbed nanospecies on the nanowire's nonlinear response and demonstrate the potential modal and wavelength division capabilities of such a coupled system.

2. Experimental details

Crystalline silver nanowires are grown using a seed-mediated chemical process following the polyol reduction of silver nitrate ($AgNO_3$) method [11,12]. This procedure yields a wide variety of single crystalline AgNW configurations with pentagonal cross-sectional shape. The diameters are ranging from 200 nm to 600 nm and the nanowires are synthesized with a wide spread of available lengths, some of which are selected for this study. A solution of AgNWs diluted in ethanol is drop-casted on a clean 22×22 mm glass coverslip having well-defined position markers. The deposited solution is dried at room temperature. The sample is transferred to an inverted microscope (Nikon, Eclipse). A schematic representation of the experimental setup is presented in Fig. 1(a). Briefly, a femtosecond laser (Coherent, Chameleon) tuned at $\lambda_0 = 808$ nm delevering 180 fs pulses at 80 MHz is focused to a diffraction-limited area on a chosen nanowire by an oil immersion high numerical aperture (N.A.) objective (100x, N.A. = 1.49). Overlapping the nanowire termination with the laser focus scatters the incident light to a broad distribution of in-plane wave-vectors enabling to phase-match the excitation with the plasmonic modes sustained by the nanowire [18]. The different linear and nonlinear optical responses are collected by the same objective and transferred by a set of relay lenses to a charge-coupled device (CCD) camera (Hamamatsu, C4742-80-12-AG) for wide-field real and Fourier plane leakage imaging [19,20]. When necessary a set of filters is placed in the optical train to reject the back-scattered laser light and to spectrally select the nonlinear response.

A scanning electron microscope (SEM) image of typical AgNWs is shown in Fig. 1(b). Figure 1(c) and Fig. 1(d) are close-up views of the terminations indicated by the white boxes in Fig. 1(b). The high resolution transmission electron microscope (HRTEM) image of Fig. 1(e) features the lattice fringes revealing the crystal arrangement. Applying a fast Fourier transform confirms the periodicity of the crystal (see inset).

While flat terminations impose specific incident polarization conditions to excite particular SPP modes, spherical-like terminations allow the excitation of multiple SPP modes regardless of the polarization [9,21]. Furthermore, the excitation of different plasmon modes may also be facilitated by the inhomogeneous distribution of the field components inside the focus [22]. In our experiments the incident polarization is kept along the major axis of the nanowire (longitudinal) where the coupling to SPP shows to be more efficient. Generally speaking, large diameter silver nanowires with a section of a few hundreds of nanometers can support plasmonic modes of different natures. The first mode is the fundamental mode bound at the surface, which is characterized by an effective index larger than that of the substrate, here $n_{\text{eff}}>1.5$. The second family of modes are higher-order modes with lower effective indices. In a leakage radiation microscope equipped with a high NA aperture, these SPP modes are radiatively loosing part of their energy into the substrate, which can then be collected to form an image of the SPP distribution [20,23]. This simple plasmonic modal landscape is modified by the cross-sectional geometry and the standardized use of the underlying substrate due to the substrate-induced hybridization of SPP modes [20,24,25]. Cross sections with sharp edges lead to field localization at the edges and corners. As the cross-sectional size is reduced, hybridization is favored and gives rise to a new and reduced set of supported modes [21]. The nanowires considered here exhibit a clear pentagonal cross-section [26] with an upper vertice distinguishable in the SEM images of Fig. 1(c), (d).

In this work, we investigate a population of nanowires characterized by a distribution of sections inherent from the chemical synthesis. Broadly speaking, one may split the section in

Optics EXPRESS

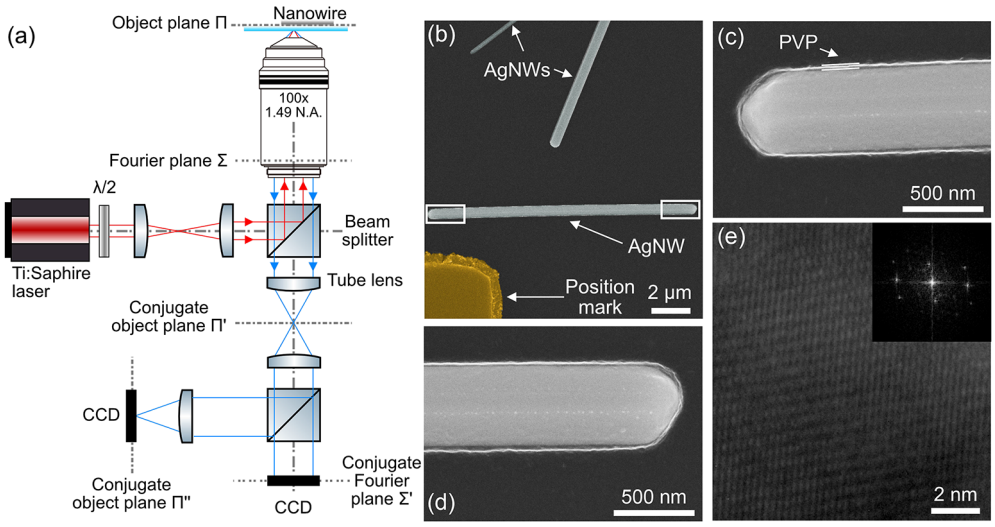

Fig. 1. (a) Experimental setup. A NIR pulsed laser is tightly focused by a high N.A. objective. The same objective also collects the optical response. A set of relay lenses allows Fourier and real plane imaging on CCD cameras. A set of filters spectrally selects the different optical responses emitted by the nanowire. Distances are not at scale. (b) SEM micrograph of typical AgNWs. (c) and (d) are closed up views of the extremities of the AgNW indicated in (b). The AgNW diameter is around 530 nm and the thin layer of polyvinylpyrrolidone (PVP) surfactant covering the AgNW is visible on the micrographs. (e) High-resolution transmission electron micrograph showing the atomic structure of the synthesized silver nanowires and the corresponding Fourier transform pattern.

two distributions. A first one allowing only the existence of the fundamental mode and roughly encompasses nanowire's diameters below 150 nm [20]. All other higher-order modes are at cut-off. The second distribution gathers larger diameters, where higher-order (leaky) modes co-exist with the bound mode.

3. Real-plane nonlinear photoluminescence distribution: effect of SPP modal pumping

Starting with the fundamental bound mode, Fig. 2(a) shows a wide-field image taken at the laser wavelength when a selected AgNW is excited. This nanowire is labeled as nanowire #1. Here, the focal spot overlaps the AgNW left extremity and is seen as an intensity-saturated region. The presence of a dimmer intensity at the distal end indicates the excitation and propagation of the surface plasmon bound mode at λ_0. The plasmon propagates along the nanowire and scatters out to free-space photons at the termination, which is a distinctive signature of the mode existence [27]. Tightly confined at the nanowire-glass interface, this mode has higher effective refractive index than the substrate. Therefore, it can only be detected in the far-field by scattering at surface impurities such as adsorbates. Some weak SPP scattering can be observed along the nanowire as dim fringes present along the nanowire. The fringe pattern results from imaging artefacts due to the spherical symmetry of the objective lens and the coherent nature of the excitation.

Increasing the incident peak power ($\approx 7 \times 10^{13}$ W $\cdot$ m^{-2} at the sample) and thus the strength of the excited surface plasmon triggers the generation of a nonlinear photoluminescence (N-PL) response in the nanowire #1. N-PL is a multifaceted process arising from different underlying absorption and emission mechanisms [28]. On the one hand, the pulsed excitation of the metal creates an out-of-equilibrium electron distribution [29]. The thermalization dynamics of the

Optics EXPRESS

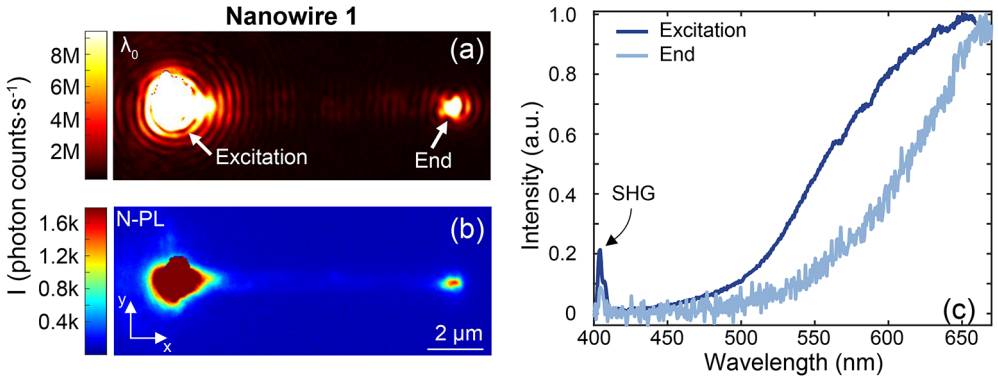

Fig. 2. (a) Wide-field image of the intensity distribution of the bound mode excited in a 9 μm long AgNW (nanowire #1). (b) Spectrally filtered image of the N-PL emitted at λ<700 nm by the nanowire. The color range saturates the images at the excitation area to reveal the weaker signals produced along the nanowires and at the distal ends. (c) Normalized spectra of the nonlinear response generated at the excitation and distal end. λ>700 nm are removed from the detection path due to the filter set utilized to reject the laser line and Raman contributions from the substrate.

distribution allows the electrons to reach high enough temperatures, which may radiate in the NIR and visible following Planck's law [30,31]. On the other hand, experimental evidence suggested an interband multi-photon absorption process taking place [32]. Electrons in the *d*-band of the metal are promoted to higher levels in the *sp*-band by sequential photon absorption events [33]. Eventually, excited electrons will recombine with holes in the *d*-band by emitting a photon. This process was identified for Au, but not systematically studied for Ag nanostructures. In this report, we do not attempt to identify the emission mechanism giving rise to N-PL. We simply use this signal as an observable supporting our claims.

Such a nonlinear emission is displayed in Fig. 2(b) where the image captures the spectrally integrated N-PL emitted at λ<700 nm and excludes the excitation wavelength and possible second harmonic generation (SHG). Besides the expected strong nonlinear response visible at the excitation area (left), there is remarkable N-PL emission at the distal end. This distal N-PL response is mainly a consequence of the localized electromagnetic enhancement provided by the end face [12]. Another contributor may also be secondary plasmons launched by the local N-PL generated at the excitation site, propagating in the nanowire and being scattered out by the end-face nanowire [34,35]. However, this contribution is expected to be weak compared to the enhancement of the pump plasmon at the extremity because of the low efficiency of the overall process, which includes N-PL generation and subsequent coupling probability to the modal structure as well as the large propagation loss at play in the considered N-PL wavelength coverage [9]. The weak N-PL response detected along the nanowire is emitted from its surface and results from the optical pumping of the material by the propagating bound SPP mode [36]. Compared to previously reported delocalized nonlinear emission occurring in top-down fabricated nanowires [34–36], the small intrinsic roughness of the crystalline AgNWs reduces momentum transfer all along the nanowire and the largest N-PL emission is mostly confined at the excitation and distal ends.

Figure 2(c) displays the spectra of the up-converted emission at the two extremities of the nanowire #1. Both N-PL spectra show the characteristic tail-like shape vanishing at decreasing wavelength. A weak coherent response is revealed at λ = 404 nm corresponding to the second-harmonic generation (rejected on the images). The spectral nature of the N-PL is linked to the equilibrated temperature of the hot electron distribution created by the ultrafast laser pulse and

Optics EXPRESS

the excitation of the SPP. The distal end of the AgNW features a depleted spectral content of the low-wavelength region compared to the excitation end. This is explained by the comparatively lower electron temperature reached at the distal end due to the loss of transmitted SPP pumping power at λ_0 during its propagation [34,37]. As pointed out above, a small portion of the emission at this location may arise from secondary N-PL plasmons scattering out. Given the dispersive nature of the nanowire, shorter wavelength plasmons suffer higher propagation losses and therefore may contribute also to the observed spectrally-depleted emission at the distal end of the nanowire.

Now, taking advantage of the inhomogeneous field components inside the laser focus, we slightly change the position of the extremity of nanowire #1 in order to excite higher-order leaky modes. Basically, controlling the lateral overlap between the extremity of the nanowire and the optimal focal field distribution enables a preferred excitation of the bound mode or leaky modes [22]. Since the leaky modes have smaller effective refractive indexes than the substrate, they can be detected by leakage radiation microscopy [38]. Indeed, the resulting leakage image taken at λ_0 is shown in Fig. 3(a). The two bright parallel lines at the lateral edges of the nanowire are the signature of the leaky nature of the mode. The plasmon propagation may be extracted by plotting the lateral SPP intensity taken along the two bright lines as shown in the semi-logarithmic graph of Fig. 3(b). The data follow a linear decaying trend indicative of the exponential attenuation of the surface plasmon. An exponential fit provides the distance after which the mode intensity I_{spp} has decayed to $1/e$, i.e. the propagation length L_{spp} of the mode: [39]

$$I_{spp} = I_0\, e^{-x/L_{spp}} \tag{1}$$

where x is the distance along the AgNW and I_0 is the initial intensity of the plasmon at the coupling site. The fit gives $L_{spp} = 2.3\ \mu$m in both data sets in close similarity with previously reported values [20,25].

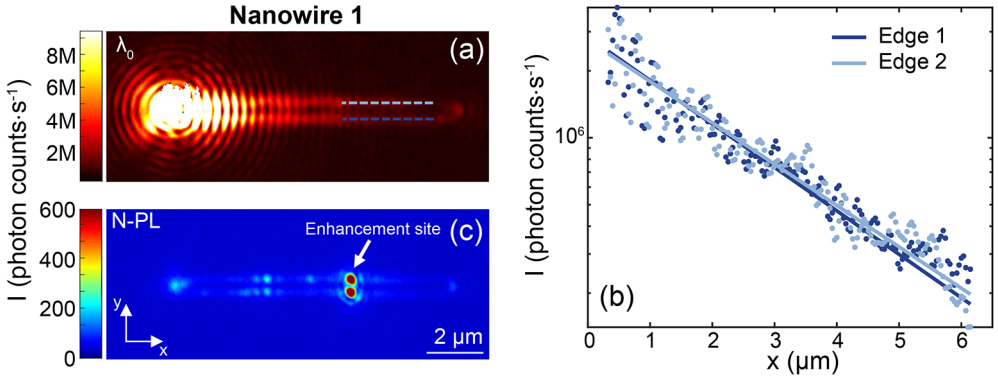

Fig. 3. (a) Wide-field image of the intensity distribution of the leaky mode excited in a 9 μm long AgNW (nanowire #1). (b) Semi-log plot of the intensity profile along the two bright lines at the edges of the nanowire as indicated in (a) by the light and dark blue dotted lines. (c) Spectrally filtered image of the N-PL emitted at λ<700 nm by the nanowire. The N-PL distribution is dominated by hot-spots at a particular locations defined by nanoparticle adsorbates.

We switch now to the nonlinear response generated when the laser intensity is increased (Fig. 3(c)). Pumping the AgNW with a leaky mode leads to very different behaviors that are systematically observed in all the investigated nanowires. Firstly, the excitation area (left end), which concentrates the vast majority of the incident power, surprisingly shows a weaker nonlinear emission compared to the excitation condition of the bound mode (Fig. 2(b)). This reduced

Optics EXPRESS

nonlinear response at the excitation input is probably linked to the slight displacement of the nanowire's position within the focus introduced to favor coupling to the leaky mode. This results in a weaker N-PL generation compared to the optimum overlap. Such a weak emission strengthens the hypothesis of the surface plasmon at the pump wavelength as the main origin of the N-PL delocalization. Secondly, the N-PL distribution along the nanowire bears a strong resemblance with the leaky mode at λ_0, whose emission is located at the edges. This suggests that the N-PL distribution is linked to leaky modes excited within the N-PL continuum. This situation is vastly different from the bound mode pumping where N-PL is emitted via a surface effect, and does not exist as a mode of the structure. Thirdly, the intensity of the N-PL is here dominated by local hot-spots at adsorbates (see white arrow as an example) which are not easily observed with the bound mode imaging neither at the pump wavelength (Fig. 2(a)) nor at its corresponding N-PL distribution (Fig. 2(b)), in spite of being the same nanowire.

The N-PL response at the hot-spots may be arising from a simple scattering of the underlying propagation of an upconverted spectral continuum of surface plasmons excited by the laser and launched at the left hand side of the nanowire. We believe that this is weak contributor to the signal. Rather, we argue that the strong responses observed at the hot-spots are produced by a local enhancement of the plasmon field transported at the pump wavelength.

Our argumentation is based on the following discussion: Let us assume for the sake of the argument that the coupling efficiency of the focal fields to a surface plasmon at the pump wavelength is of the same order of magnitude as the coupling efficiency of the locally generated N-PL at the excitation end to a continuum of plasmons. The ratio between the strength of these secondary plasmons and the strength of the plasmon developing at the fundamental wavelength would be equal to the N-PL generation yield. Such extrinsic yield was reported to be as low as 10^{-10} in earlier publications [e.g. [40]] and we estimate a similar value by normalizing the N-PL photon counts measured at the excitation site by the number of incident pump photons. There is thus a huge difference on the efficiency of the evoked mechanisms to explain the local N-PL responses observed, favoring thereby the vision of a local enhancement of the pump plasmon field by the presence of adsorbates. Another hint supporting this argument is that scattering of a plasmon continuum is expected to exponentially decay with the distance separating the location of the hot-spots to the excitation end. Within the wavelength range of the upconverted N-PL photons the surface plasmon propagation distance is lower than that of the fundamental plasmon, here measured as $L_{spp} = 2.3\ \mu$m. This dependence is not observed experimentally. Instead, Fig. 3(c) (and others discussed below) shows that the N-PL signal at the strongest enhanced site is actually larger than at the focus and thus cannot be understood by a mere scattering of an underlying upconverted plasmon continuum. Finally, scattering of the surface plasmon field by an adsorbate decorating the surface of the nanowire is not always an efficient out-coupling mechanism. Good examples are illustrated in Fig. 2(a) and Fig. 3(a) where the presence of particles does not drastically affect the propagation of the bound and leaky modes.

The explanation fundamentally lies on the near-field cross-sectional distribution of the plasmonic modes. The generation of hot-spots is linked to the enhancement of the SPP fields produced by an electromagnetic interaction with surface adsorbates [41] which, in this case, are formed by residues of the synthesis decorating the nanowire. SEM characterization of the studied nanowires confirms the presence of adsorbed nanoparticles at the location of the enhancement sites. Figure 4 shows a set of images with different particle-nanowire configurations randomly obtained during chemical synthesis. The strength of the enhancement can be linked to the orientation of the field polarization and the presence of a small gap separating the two metal surfaces [42,43]. The junctions observed on SEM images are not trivial but contribute enormously to the build up of the optical fields and the efficient generation of local nonlinear sources. Therefore, the intensity of N-PL signal at particular hot-spots is essentially defined by the geometrical factor of the junction and the plasmon modal characteristics.

Optics EXPRESS

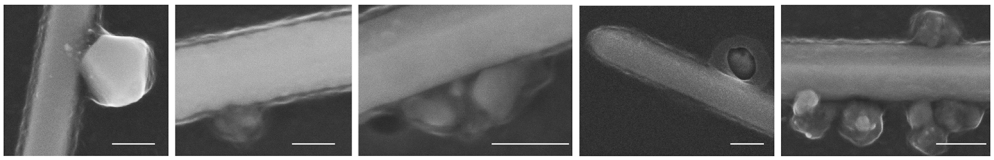

Fig. 4. SEM images of adsorbed nanoparticles on silver nanowires acting as hot-spots for the enhancement of nonlinear optical responses and routers for exciting the family of SPP modes supported by the nanowire. Scale bars are 200 nm.

To confirm this hypothesis, Fig. 5 shows the computed cross-sectional views of the field intensity distributions characterizing the different guided surface plasmon modes supported by a 500 nm wide pentagonal AgNW at $\lambda_0 = 808$ nm. The nanowire is surrounded by air ($n = 1$) and lying on a glass substrate ($n = 1.5$). The modes are identified and computed by a commercial mode solver (COMSOL Multiphysics, RF module) and a homemade (Green's dyad) method. The computation provides the complex effective index of the guided modes $n_{\text{eff}}^{\sim} = n_{\text{eff}} + in''_{\text{eff}}$ and their field distribution. Details can be found in [20,44].

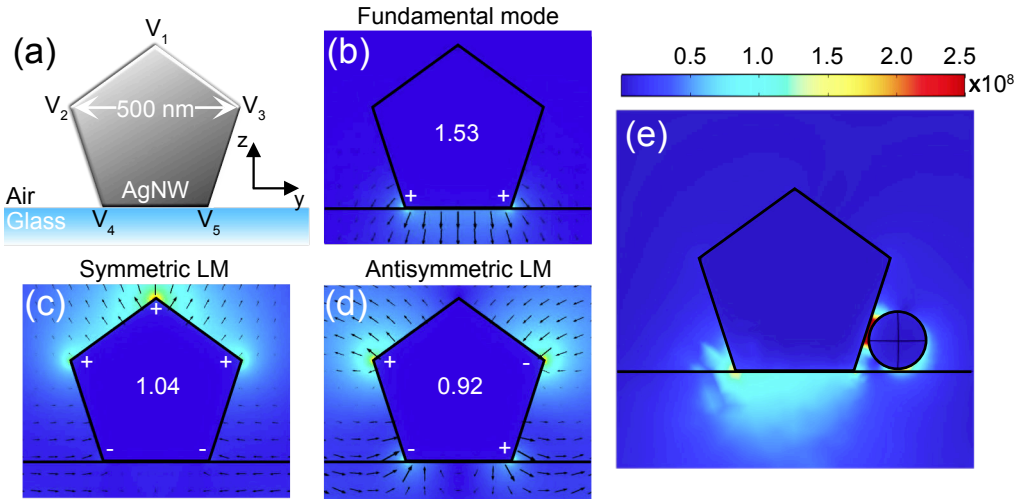

Fig. 5. Electric field intensity distributions of the plasmonic modes supported by a 500 nm wide AgNW lying on a glass substrate and excited at $\lambda_0 = 808$ nm. (a) Schematic representation of the air-nanowire-substrate system. The corners of the nanowire are labeled as V_i ($i = 1$ to 5) for easier identification. (b), (c) and (d) are cross sectional intensity distributions for the fundamental bound mode, symmetric and antisymmetric leaky modes, respectively. The numbers at the center of the pentagons are the calculated effective indexes while the plus and minus signs highlight the polarity of the charge density distribution. The arrows represent the orientation of the electric field. (e) Intensity distribution of the electric field when the bound mode interacts with a 150 nm spherical Ag nanoparticle placed on the nanowire's side. A 5 nm gap is introduced to mimic the presence of the surfactant layer.

The fundamental mode features an intensity distribution confined to the glass-AgNW interface and principally at corners V_4 and V_5 (see Fig. 5(b)). Its effective index is estimated at $n_{\text{eff}}(\text{BM}) = 1.53$. Two additional modes are sustained by the nanowire as shown in Fig. 5(c) and (d). Previously reported as symmetric (longitudinal, SLM) and anti-symmetric (transverse, ALM) modes according to the symmetry of the charge distribution [25], these modes are leaking radiation into the substrate, and their effective indexes are $n_{\text{eff}}(\text{SLM}) = 1.04$ and $n_{\text{eff}}(\text{ALM}) = 0.92$ for the

Optics EXPRESS

symmetric and antisymmetric modes, respectively. In clear difference with the bound mode, the field intensity distribution of the symmetric leaky mode is mainly found at the summit corner of the nanowire V_1 and to a minor extent in V_2 and V_3. For the antisymmetric leaky mode the field concentrates at the two side corners V_2 and V_3, but is also present at the corners in contact with the substrate.

Hence, if an adsorbate would be situated on the nanowire's upper surface, it would act as a scattering center for the leaky modes, but would not affect much the propagation of the bound mode as its field distribution is protected by the interface with the substrate. Furthermore, the orientation of the leaky mode field lines (arrows in Fig. 5(c,d)) promotes the creation of strong field-enhanced region located in the interstice separating the coupled system [42,43], which is expected to be a strong contributor to the generation of a local N-PL secondary source. This is experimentally shown in Fig. 3(c). In an attempt to vizualize the occurrence of a field enhancement promoted by the adsorption of a nanoparticle we show in Fig. 5(e) the distribution of the field intensity when a 150 nm spherical nanoparticle interacts with the bound mode propagating in the nanowire. We take into account the presence of the surfactant layer observed in the SEM images by introducing a 5 nm gap between the surface of the nanowire and the nanoparticle. Clearly, the simulation unambiguously reveals the presence of a local field enhancement in the gap region. Because N-PL is a nonlinear process, this localized enhancement at the pump wavelength significantly increases the strength of the up-converted signal. The magnitude of the enhancement evidently depends on many different parameters including the precise position of the nanoparticle, its geometry as well as the nature of the propagating mode. A systematic analysis of all these dependencies goes beyond the present reports.

4. Fourier plane analysis of the N-PL maps

Although real-space imaging gives useful information about the spatial distribution of the light scattered by the nanowire, it does not reveal the complete set of information available. Conveniently, the principles of Fourier optics allow mapping of the wave-vector distribution (k_x, k_y) in a plane conjugate to the back focal plane of the objective [19]. Figure 6 shows the Fourier planes at the pump and N-PL wavelengths corresponding to the bound and leaky mode pumping of the nanowire #1 presented above. Object plane images are again displayed at the top for guidance.

When the bound mode develops in the nanowire (Fig. 6(a), (b)), the two corresponding Fourier planes exhibit considerably different patterns given the intrinsic dissimilarities of their fundamental underlying emission mechanisms. At λ_0, the interference fringes extending all along k_y/k_0 arise from the coherence of the process and the finite length of the nanowire. The fringes become less clear as k_x/k_0 decreases. This pattern is generally well reproduced by a chain of dipoles oscillating at the pump frequency with a defined phase mimicking plasmon propagation [22,45]. In contrast, the N-PL Fourier plane exhibits no interference (N-PL is an incoherent process) and the emission is azimuthally restricted by the nanowire into two lobes oriented with the reciprocal propagation axis. Essentially, the N-PL generated at the excitation end, which represents the strongest response (see upper panel in Fig. 6(b)), is affected by the presence of the nanowire which acts as an antenna by orienting the emission in a direction along its major axis [46]. The vertical asymmetry towards $-k_y/k_0$ is due to a residual misalignment of the laser spot with respect to the center of the AgNW.

In Fourier space, a leaky mode is easily recognized by the presence of a thin straight line transverse to the reciprocal direction of propagation as exemplified in Fig. 6(c). It results from the strong confinement of the mode in the y-direction and thus contains a broad wave-vector distribution in k_y [22]. The position of the line on the k_x axis gives the effective index of the SPP mode and the full width at half maximum (FWHM) encodes the propagation length and thus losses. More precisely, the intensity of leakage radiation in k-space can be described by a Lorentzian

Optics EXPRESS

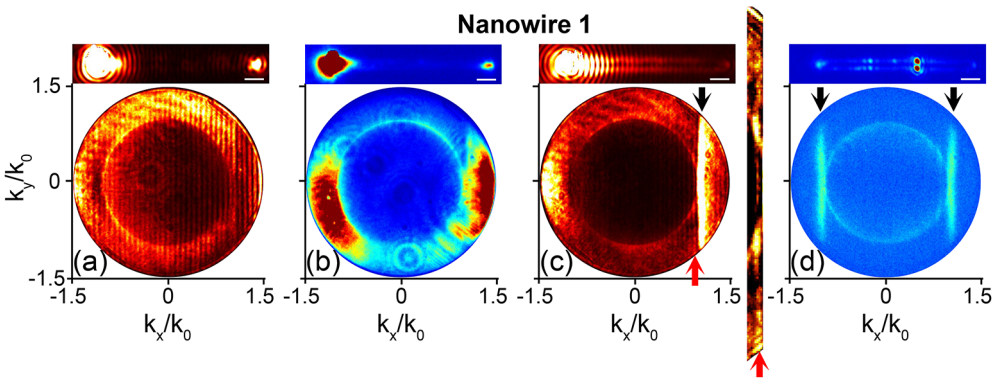

Fig. 6. Fourier planes of the light collected at the pump wavelength and across the N-PL spectrum for SPP developing in the 9 μm long Nanowire #1 for two modal pumping conditions. Bound mode excitation: (a) Wave-vector distribution produced by the bound mode excitation at λ_0, (b) Corresponding wave-vector distribution measured across the N-PL spectral range. The diffraction rings in (a) and (b) are scattering residues present on the relay lenses and are not related to the mode. Leaky mode excitations: (c) Wave-vector distribution measured at λ_0, (d) Wave-vector distribution measured across the N-PL spectral range. The zoomed frame in (c) is a higher contrast image at $k_x/k_0 \approx 0.93$ revealing the presence of the anti-symmetric leaky mode pointed by a red arrow. The upper panels are the corresponding object plane images. Scale bars are 1 μm.

distribution [38,44]. Here, the Fourier plane clearly exhibits a line at $+k_x/k_0 = n_{\text{eff}} = 1.05$ (black arrow) in close agreement with the calculated symmetric leaky mode of Fig. 5(c). Additionally, a weaker maximum of intensity is detected at $n_{\text{eff}} = 0.93$ (see zoomed frame taken at the red arrow location) and hints at the presence of the anti-symmetric leaky mode. The presence of a faint fringe system towards the $+k_x$ semi-plane signals a residual bound mode propagating in the nanowire.

Unexpectedly, the Fourier plane of the corresponding N-PL emission displayed in Fig. 6(d), features two vertical lines symmetric with respect to $k_x/k_0 = 0$. This is the signature of propagating plasmons transported in the $+x$ and $-x$ directions with nearly equal amplitudes. The explanation is as follows. The leaky plasmon propagating at the pump wavelength λ_0 travels in the $+x$ direction after being launched at the left extremity of the nanowire. A reflection of the SPP mode at the right termination may occur, but the reflection coefficient is usually low [47–49] and would not account for the balanced signal amplitude observed in Fourier space. However, this pump leaky plasmon mode promotes the generation of a secondary nonlinear continuum at a nanoparticle accidentally decorating the nanowire. In line with the discussion of Fig. 5, the electric field lines attached to the leaky mode favor the creation of a local enhancement site in the gap between the adsorbate and the nanowire surface, which acts as a secondary N-PL local source. In the subsequent step, the local continuum couples equally to a new set of modes propagating and leaking in the forward ($+x$) and backward ($-x$) directions as demonstrated by the emission diagram. The efficiency of the coupling process is given by the distribution of in-plane wave-vectors of the secondary N-PL source. As this source is localized, the wave-vector distribution is very broad and contains the necessary wave-vectors for launching a spectrally wide continuum of leaky SPPs.

Remarkably, the nanowire-particle system performs simultaneously wavelength and wave-vector conversions and provides a mean to populate the complete modal structure of the nanowire. From pump leaky plasmon modes transported in one direction (input), the system creates a new

Optics EXPRESS

set of plasmon modes excited within the wavelength range of the N-PL and propagating in two opposite directions.

To summarize the mechanisms discussed so far, Figs. 7(a,b) schematically depict the excitation, propagation and emission processes taking place in the case of bound and leaky mode excitations in the nanowire #1. In Fig. 7(a), the location of the adsorbate does not affect the propagation of the bound mode at the pump wavelength. The N-PL generated under this excitation modality is strong at the extremities. It is also distributed along the nanowire and results from a surface effect locally promoted by the pump plasmon. When pumping the nanowire with a leaky mode as depicted in Fig. 7(b), the nanoparticle introduces a visible disturbance of the mode recognized in the leakage images. The effect of the nanoparticle is best observed on the N-PL distribution. The field-enhancement created by the interaction with the pump field generates a strong secondary N-PL source, which subsequently couples to leaky modes propagating in the nanowire away from the nanoparticle.

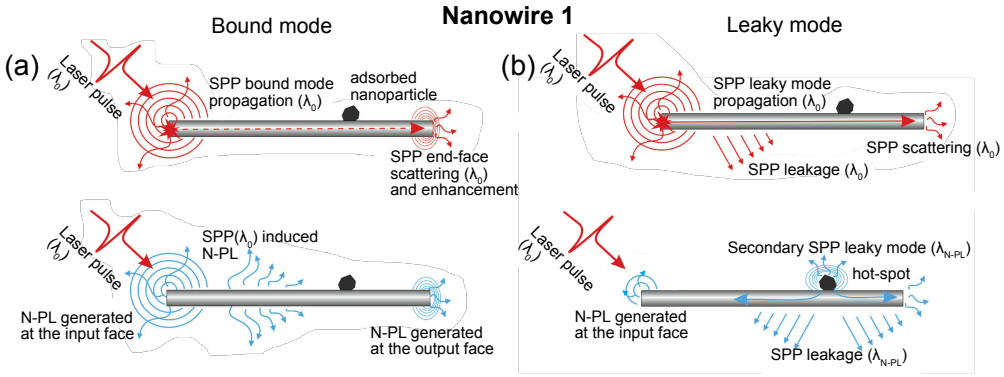

Fig. 7. Sketches of the linear and subsequent nonlinear secondary excitation, propagation and emission processes occurring in the nanowire #1 studied above when the (a) bound mode and (b) leaky mode are excited.

5. Additional modal conversion processes enabled by terminations and defects

In the following, we confirm the robustness of these conversions and present interesting additional modal switching capabilities that could be tailored by adjusting the position of the enhancement site and the thickness of the nanowire. Precisely defining the interaction volume of the nanowire-particle junction and the activation of the hot-spot by the excited plasmon mode in the nanowire is a difficult task: the circumstantial nature of the position, orientation and morphology of the enhancement sites hamper a fair comparison between the studied junctions. The present work should be seen as a starting point to engineer design rules for the next generation of man-made arrangements.

Figure 8(a) displays a 6 μm long AgNW labeled as nanowire #2 in which the bound mode is excited. An optical transmission image of the nanowire completes the figure at the top. The parallel fringes in the corresponding Fourier plane presented in Fig. 8(b) corroborate the excitation of a fundamental SPP mode transported towards the $+x$ direction. The N-PL distribution of this particular nanowire (Fig. 8(c)) features an intense response of the right termination despite being excited at its left extremity. Akin to Fig. 6(d), the N-PL emission at this location acts as a secondary source which can trigger the excitation of additional wavelength-converted SPP modes in the nanowire. Because the N-PL radiates at the right end-face, only SPP modes propagating in the $(-x)$ direction may develop. The vertical line at $-k_x/k_0$ in the N-PL Fourier plane of Fig. 8(d) confirms the leaky nature of these secondary modes. Additional features in the $-k_x/k_0$ half of the

Optics EXPRESS

Fourier plane come from the localized emission of the enhancement site. Nanowire-nanoparticle junctions have shown directional emission [50] in addition to the already mentioned antenna effect steered by the nanowire. In this example, the conversion occurs from the fundamental (bound) mode at λ_0 propagating towards $+x$ to counter propagating ($-x$) higher-order (leaky) modes with a large spectral content, i.e. we observe a modal division where a bound mode is converted to spectrally-broad secondary leaky modes propagating in opposite direction. Clearly, the precise position of the enhancement site plays a key role in this activation, which in this case, is promoted by the termination itself. Figures 8(e), (f) summarize the analysis by showing schematic representations of the linear bound mode excitation, propagation and subsequent hot-spot activation and conversion into counter-propagating N-PL leaky modes.

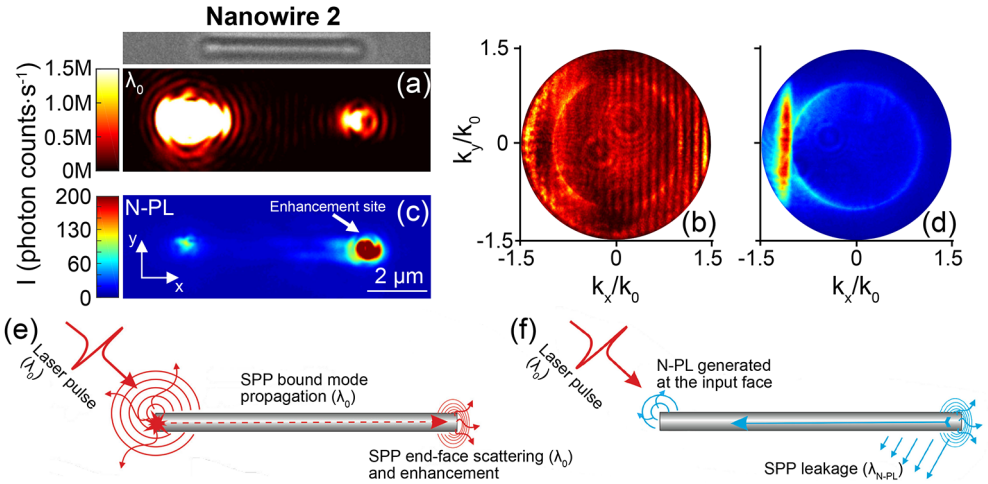

Fig. 8. Bound to leaky mode conversion in a 6 μm AgNW. (a) Intensity distribution in the nanowire when the SPP bound mode is excited. The laser is placed at the left end. A bright field transmission image of the nanowire is displayed at the top. (b) Fourier plane of the situation shown in (a). (c) Corresponding image of the N-PL distribution (λ<700 nm) and (d) its Fourier plane. Schematic sketches showing (e) the linear bound mode launched in the nanowire #2 and (f) the strong N-PL response at the termination which couples to secondary leaky modes within the N-PL spectral content.

As reported by Jia and co-workers [25], multiple plasmonic modes can be simultaneously excited under certain polarizations of the excitation laser. However, such approach is not convenient for advanced functions and practical applications which require local and direct control of the supported plasmonic modes in the nanowire [8,51]. Alternatively, this single- to multi-mode conversion can be readily achieved by introducing a local structural defect in a thick enough nanowire and by activating its broadband nonlinear response as demonstrated in the following example. Figure 9(a) displays the intensity distribution at λ_0 when a leaky mode propagating in the x-direction is excited on the AgNW labeled here as nanowire #3. The Fourier plane of Fig. 9(b) reveals the typical line and signature of the mode at $+k_x/k_0 \approx 1.05$. Even though an additional leaky mode may be possibly excited, the absence of beating in the intensity distribution along the lateral edges of the nanowire suggests that its contribution is negligible. An abrupt loss of the leakage signal is observed close to the distal end of the nanowire and is indicated by the pointing white arrow in Fig. 9(a).

Looking now at the resulting N-PL distribution, Fig. 9(c) features two intense emission spots. One positioned at the excitation location and a second, equally intense, located at the site identified by the dim region in Fig. 9(a). At this point of the discussion, we recall the analysis about the

Optics EXPRESS

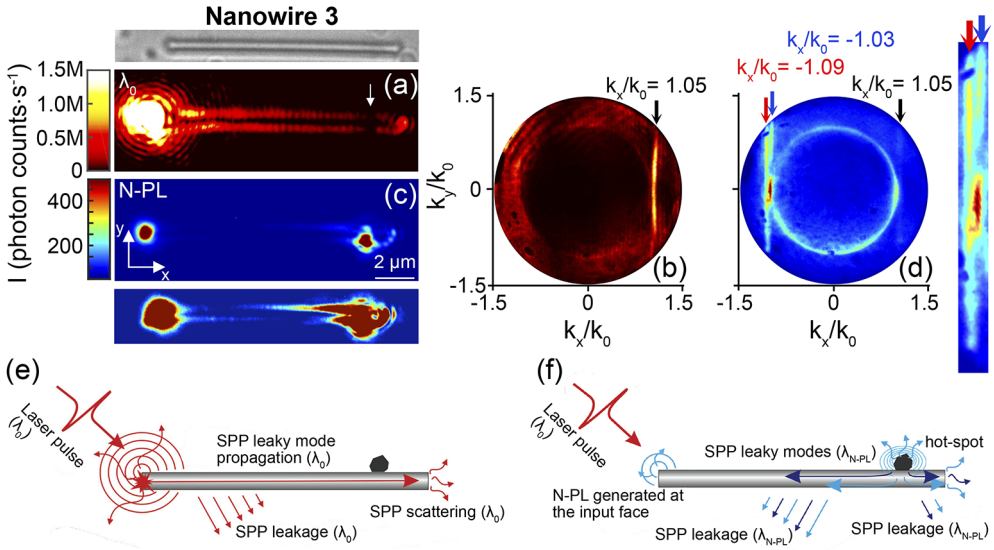

Fig. 9. Single to multi-mode conversion in a 12 μm long AgNW. (a) Wide-field image of the pump leaky mode excited by placing the laser beam at the left end of the nanowire. Top: A bright-field transmission image of the same nanowire. (b) Corresponding Fourier plane image of the leakage at λ_0. (c) Corresponding N-PL emission (λ<700 nm) for the excitation condition shown in (a). The image is saturated at the bottom frame to highlight the emission located on the edges. (d) N-PL Fourier plane of (c). The frame on the right of (d) is a zoomed view of the area showing the signature of two supported secondary leaky modes. (e) (f) Schematic sketches of the situations shown in (a) and (c).

efficiency of the N-PL generation at the excitation input. The N-PL intensity produced at the focus is often comparable to hot-spot responses distributed along the nanowire in spite of being directly excited by the laser (see Fig. 3(c),8(c),9(c)). On the one hand, nanoparticle-nanowire junctions provide greater enhancement factors than any other locations [12] as confirmed by the simulation already shown in Fig. 5(e). On the other hand, the N-PL yield is given by the specific overlapping of the pump optical fields with the nanowire extremity as well as the morphological particularities of the end facet of the nanowire. Essentially, the focus position providing an optimal excitation of the leaky SPP mode does not necessarily match that of the maximum local N-PL generation.

Increasing the contrast of the nonlinear real plane image (see bottom frame of Fig. 9(c)), reveals a beating of the intensity along the structure which alternates between the upper and lower edge of the AgNW with a period approaching the length of the nanowire. This is in close similarity with the zigzag pattern exhibited when several plasmonic modes superpose [25,52]. The corresponding N-PL Fourier plane of Fig. 9(d) confirms the presence of several secondary leaky modes. Firstly, by the single line at $+k_x/k_0 \approx 1.05$ and secondly by the two straight lines in the $-k_x$ semi-plane at specifically $-k_x/k_0 \approx -1.03$ and $-k_x/k_0 \approx -1.09$ (see zoomed frame on the right hand side of the Fourier plane). The contribution of $+k_x/k_0$ is weaker than the two modes observed at $-k_x/k_0$ because the defect is placed at a few micrometers from the right termination. The mode cannot fully develop in this short nanowire section [20]. In this example, the enhancement site induces a modal switching, from a single leaky mode at the pump wavelength ($+x$-direction) to multiple up-converted secondary leaky modes launched by the defects and propagating in both directions. Finally, Fig. 9(e), (f) sketch the linear leaky mode excitation and the conversion to multiple nonlinear leaky modes mediated by the nanowire-nanoparticle junction of nanowire #3.

Optics EXPRESS

Now, the beating period Λ_{beat} observed in Fig. 9(c) is related to the propagation constants of the two modes and thus depends on the nanowire parameters such as width and environment medium. In terms of effective indexes of the leaky modes just extracted above and considering for simplicity an intermediate wavelength within the N-PL detected range at $\lambda = 600$ nm, the beating writes [8]

$$\Lambda_{beat} = \frac{\lambda}{n_{eff}^{(1)} - n_{eff}^{(2)}} \approx 10\ \mu m \tag{2}$$

which is not too far from the observed pattern of Fig. 9(c). Nevertheless, this value must be cautiously examined and considered only as a reference. The complete set of plasmon modes developing in the AgNW and spanning throughout the N-PL wavelengths is not being taken into account here. The effective indexes are numerically calculated in Fig. 10 for $\lambda = 600$ nm and compared with the values obtained in the experimental Fourier plane of Fig. 9(d), which measures the signal over the N-PL spectral range (λ<700 nm). The blue curve in Fig. 10(a) shows the calculated two-dimensional local density of states (2D-LDOS) in wave-vector space and is a direct way to represent the eigen modes and their effective indexes.

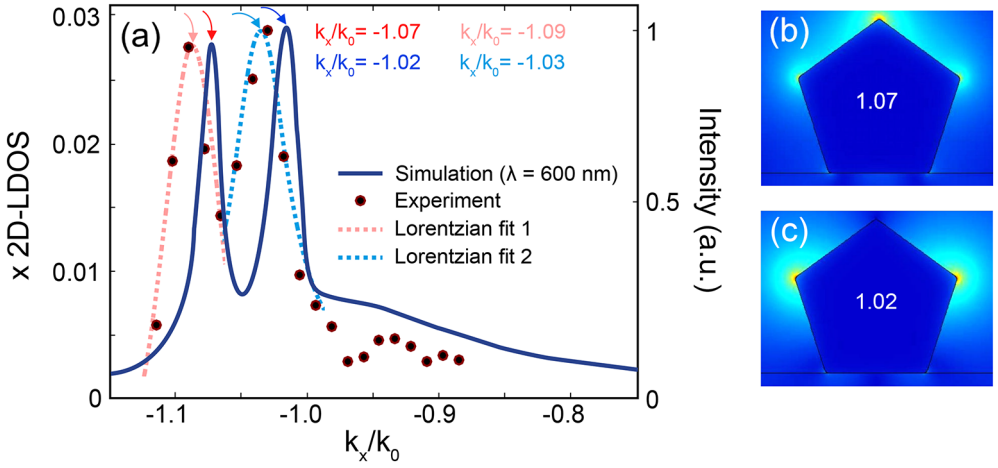

Fig. 10. (a) The blue curve represents the calculated 2D-LDOS for a 500 nm wide pentagonal AgNW at $\lambda = 600$ nm. Points indicate the profile extracted from the Fourier plane of Fig. 9(d). The profile is completed with Lorentzian fits (dashed curves). Colored arrows point to the location of the peaks. (b) and (c) display the cross-sectional field distribution of the two leaky modes calculated at $\lambda = 600$ nm.

Two modes are present in the simulation at $k_x/k_0 = -1.07$ and $k_x/k_0 = -1.02$. The analysis is completed by the cross-sectional field distribution of the two modes in Fig. 10(b) and 10(c) showing similar patterns to those of Fig. 5(c) and 5(d) respectively.

Let us now compare the simulations for a single wavelength (blue curve, $\lambda = 600$ nm) and the profile of the experimental Fourier plane of Fig. 9(d) which comprises the entire N-PL spectral range (black points, λ<700 nm). The data points are fitted by two Lorentzian fits (dashed curves). The experiment reveals wider peaks compared to the simulation as a consequence of the broad spectral content of the N-PL and the increased losses associated with lower wavelengths. This confirms the propagation of multiple secondary leaky plasmons launched at different wavelengths, propagation lengths and effective indexes. The shift between the eigen mode indexes and the measured data is explained by the difference between the simulated section and the real nanowire's dimensions [20], which are not precisely known.

Optics EXPRESS

6. Conclusions

We show that modal surface plasmon conversions and nonlinear broad-band wavelength conversion may be promoted by silver plasmonic nanowires decorated by adsorbed nanoparticles. The excitation of the coupled nanowire–nanoparticle system by a pump plasmon mode locally triggers an enhanced electromagnetic field acting as a secondary source emitting a spectrally-broad nonlinear photoluminescence. The confined nature of this secondary source enables the excitation of additional sets of plasmonic modes sustained by the nanowire and not present at the pump wavelength. We find that modal switching is sensitive to the characteristic of the pumping mode and its particular field distribution.

Modal and wavelength conversions are crucial for the design and implementation of plasmonic circuits. The different spatial distributions of the nonlinear responses discussed here may be deployed advantageously. Evidently, modal and wavelength conversion efficiencies at the adsorbed species depend on the precise geometry of the spot generating the nonlinear continuum. Future investigations will focus on the effect of the particle size and position on the optical responses as well as on quantifying the coupling efficiency and modal conversion. The wave-vector distribution and polarization state of the secondary emission are key aspects to be further explored. Our work serves as an initial guide to engineer design rules in the next generation of devices. Controlling the different processes by for instance fabricating man-made nano-scale scatterers at precise positions may enable a greater degree of switching and routing tasks in nanowire-based network devices. More complex systems made out of multiple branched nanowires are also conceivable and would provide access to full directional wavelength and modal multiplexing.

Funding. Région de Bourgogne Franche-Comté; Délégation Régionale à la Recherche et à la Technologie; Centre National de la Recherche Scientifique; EIPHI Graduate School (contract ANR-17-EURE-0002); European Regional Development Fund; Indo-French Centre for the Promotion of Advanced Research (project No. 5504-3); Conseil régional de Bourgogne-Franche-Comté (project APEX).

Disclosures. The authors declare no conflicts of interest.

Data availability. The data underlying the results of this study are available from the corresponding author upon request.

References

1. W. L. Barnes, A. Dereux, and T. W. Ebbesen, "Surface plasmon subwavelength optics," Nature **424**(6950), 824–830 (2003).
2. J. A. Schuller, E. S. Barnard, W. Cai, Y. C. Jun, J. S. White, and M. L. Brongersma, "Plasmonics for extreme light concentration and manipulation," Nat. Mater. **9**(3), 193–204 (2010).
3. Y. Fang and M. Sun, "Nanoplasmonic waveguides: towards applications in integrated nanophotonic circuits," Light: Sci. Appl. **4**(6), e294 (2015).
4. Y. Lin, X. Zhang, X. Fang, and S. Liang, "A cross-stacked plasmonic nanowire network for high-contrast femtosecond optical switching," Nanoscale **8**(3), 1421–1429 (2016).
5. H. Wei, Z. Wang, X. Tian, M. Käll, and H. Xu, "Cascaded logic gates in nanophotonic plasmon networks," Nat. Commun. **2**(1), 387 (2011).
6. J. Niedziółka-Jönsson and S. Mackowski, "Plasmonics with metallic nanowires," Materials **12**(9), 1418 (2019).
7. X. Xiong, C.-L. Zou, X.-F. Ren, A.-P. Liu, Y.-X. Ye, F.-W. Sun, and G.-C. Guo, "Silver nanowires for photonics applications," Laser Photonics Rev. **7**(6), 901–919 (2013).
8. H. Wei, D. Pan, S. Zhang, Z. Li, Q. Li, N. Liu, W. Wang, and H. Xu, "Plasmon waveguiding in nanowires," Chem. Rev. **118**(6), 2882–2926 (2018).
9. H. Yang, M. Qiu, and Q. Li, "Identification and control of multiple leaky plasmon modes in silver nanowires," Laser Photonics Rev. **10**(2), 278–286 (2016).
10. A. S. Baburin, A. M. Merzlikin, A. V. Baryshev, I. A. Ryzhikov, Y. V. Panfilov, and I. A. Rodionov, "Silver-based plasmonics: golden material platform and application challenges," Opt. Mater. Express **9**(2), 611–642 (2019).
11. Y. Sun, Y. Yin, B. T. Mayers, T. Herricks, and Y. Xia, "Uniform silver nanowires synthesis by reducing agno3 with ethylene glycol in the presence of seeds and poly (vinyl pyrrolidone)," Chem. Mater. **14**(11), 4736–4745 (2002).
12. R. Chikkaraddy, D. Singh, and G. V. P. Kumar, "Plasmon assisted light propagation and raman scattering hot-spot in end-to-end coupled silver nanowire pairs," Appl. Phys. Lett. **100**(4), 043108 (2012).
13. D. E. Chang, A. S. Sørensen, E. A. Demler, and M. D. Lukin, "A single-photon transistor using nanoscale surface plasmons," Nat. Phys. **3**(11), 807–812 (2007).

Optics EXPRESS

14. S. Viarbitskaya, A. Teulle, R. Marty, J. Sharma, C. Girard, A. Arbouet, and E. Dujardin, "Tailoring and imaging the plasmonic local density of states in crystalline nanoprisms," Nat. Mater. **12**(5), 426–432 (2013).
15. S. Viarbitskaya, A. Cuche, A. Teulle, J. Sharma, C. Girard, A. Arbouet, and E. Dujardin, "Plasmonic hot printing in gold nanoprisms," ACS Photonics **2**(6), 744–751 (2015).
16. U. Kumar, S. Viarbitskaya, A. Cuche, C. Girard, S. Bolisetty, R. Mezzenga, G. Colas des Francs, A. Bouhelier, and E. Dujardin, "Designing plasmonic eigenstates for optical signal transmission in planar channel devices," ACS Photonics **5**(6), 2328–2335 (2018).
17. D. Pan, H. Wei, Z. Jia, and H. Xu, "Mode conversion of propagating surface plasmons in nanophotonic networks induced by structural symmetry breaking," Sci. Rep. **4**(1), 4993 (2015).
18. J.-C. Weeber, A. Dereux, C. Girard, J. R. Krenn, and J.-P. Goudonnet, "Plasmon polaritons of metallic nanowires for controlling submicron propagation of light," Phys. Rev. B **60**(12), 9061–9068 (1999).
19. A. B. Vasista, D. K. Sharma, and G. V. P. Kumar, "Fourier plane optical microscopy and spectroscopy," *Digital Encyclopedia of Applied Physics* pp. 1–14 (2018).
20. M. Song, A. Bouhelier, P. Bramant, J. Sharma, E. Dujardin, D. Zhang, and G. Colas des Francs, "Imaging Symmetry-Selected Corner Plasmon Modes in Penta-Twinned Crystalline Ag Nanowires," ACS Nano **5**(7), 5874–5880 (2011).
21. S. Nauert, A. Paul, Y.-R. Zhen, D. Solis Jr, L. Vigderman, W.-S. Chang, E. R. Zubarev, P. Nordlander, and S. Link, "Influence of cross sectional geometry on surface plasmon polariton propagation in gold nanowires," ACS Nano **8**(1), 572–580 (2014).
22. M. Song, J. Dellinger, O. Demichel, M. Buret, G. Colas des Francs, D. Zhang, E. Dujardin, and A. Bouhelier, "Selective excitation of surface plasmon modes propagating in ag nanowires," Opt. Express **25**(8), 9138–9149 (2017).
23. R. Zia, M. D. Selker, and M. L. Brongersma, "Leaky and bound modes of surface plasmon waveguides," Phys. Rev. B **71**(16), 165431 (2005).
24. S. Zhang and H. Xu, "Optimizing substrate-mediated plasmon coupling toward high-performance plasmonic nanowire waveguides," ACS Nano **6**(9), 8128–8135 (2012).
25. Z. Jia, H. Wei, D. Pan, and H. Xu, "Direction-resolved radiation from polarization-controlled surface plasmon modes on silver nanowire antennas," Nanoscale **8**(48), 20118–20124 (2016).
26. P. Zhang, I. Wyman, J. Hu, S. Lin, Z. Zhong, Y. Tu, Z. Huang, and Y. Wei, "Silver nanowires: Synthesis technologies, growth mechanism and multifunctional applications," Mater. Sci. Eng., B **223**, 1–23 (2017).
27. R. M. Dickson and L. A. Lyon, "Unidirectional plasmon propagation in metallic nanowires," J. Phys. Chem. B **104**(26), 6095–6098 (2000).
28. L. Roloff, P. Klemm, I. Gronwald, R. Huber, J. M. Lupton, and S. Bange, "Light emission from gold nanoparticles under ultrafast near-infrared excitation: Thermal radiation, inelastic light scattering, or multiphoton luminescence?" Nano Lett. **17**(12), 7914–7919 (2017).
29. J. R. M. Saavedra, A. Asenjo-Garcia, and F. J. García de Abajo, "Hot-electron dynamics and thermalization in small metallic nanoparticles," ACS Photonics **3**(9), 1637–1646 (2016).
30. T. Haug, P. Klemm, S. Bange, and J. M. Lupton, "Hot-electron intraband luminescence from single hot spots in noble-metal nanoparticle films," Phys. Rev. Lett. **115**(6), 067403 (2015).
31. K. Malchow and A. Bouhelier, "Photon bunching of the nonlinear photoluminescence emitted by plasmonics metals," J. Opt. Soc. Am. B **38**(2), 576–583 (2021).
32. M. R. Beversluis, A. Bouhelier, and L. Novotny, "Continuum generation from single gold nanostructures through near-field mediated intraband transitions," Phys. Rev. B **68**(11), 115433 (2003).
33. P. Biagioni, D. Brida, J.-S. Huang, J. Kern, L. Duo, B. Hecht, M. Finazzi, and G. Cerullo, "Dynamics of four-photon photoluminescence in gold nanoantennas," Nano Lett. **12**(6), 2941–2947 (2012).
34. A. Agreda, D. K. Sharma, S. Viarbitskaya, R. Hernandez, B. Cluzel, O. Demichel, J.-C. Weeber, G. Colas des Francs, G. V. P. Kumar, and A. Bouhelier, "Spatial distribution of the nonlinear photoluminescence in au nanowires," ACS Photonics **6**(5), 1240–1247 (2019).
35. A. de Hoogh, A. Opheij, M. Wulf, N. Rotenberg, and L. Kuipers, "Harmonics generation by surface plasmon polaritons on single nanowires," ACS Photonics **3**(8), 1446–1452 (2016).
36. S. Viarbitskaya, O. Demichel, B. Cluzel, G. Colas des Francs, and A. Bouhelier, "Delocalization of nonlinear optical responses in plasmonic nanoantennas," Phys. Rev. Lett. **115**(19), 197401 (2015).
37. R. Hernandez, R. Juliano Martins, A. Agreda, M. Petit, J.-C. Weeber, A. Bouhelier, B. Cluzel, and O. Demichel, "Delocalized hot electron generation with propagative surface plasmon polaritons," ACS Photonics **6**(6), 1500–1505 (2019).
38. A. Drezet, A. Hohenau, D. Koller, A. Stepanov, H. Ditlbacher, B. Steinberger, F. R. Aussenegg, A. Leitner, and J. R. Krenn, "Leakage radiation microscopy of surface plasmon polaritons," Mater. Sci. Eng., B **149**(3), 220–229 (2008).
39. H. Raether, *Surface Plasmons on Smooth and Rough Surfaces and on Gratings*, vol. 111 of *Springer Tracts in Modern Physics* (Springler-Verlag, 1988).
40. G. T. Boyd, Z. H. Yu, and Y. R. Shen, "Photoinduced luminescence from the noble metals and its enhancement on roughened surfaces," Phys. Rev. B **33**(12), 7923–7936 (1986).
41. K.-H. Kim and Y.-S. No, "Light coupling between plasmonic nanowire and nanoparticle," J. Korean Phys. Soc. **73**(9), 1283–1288 (2018).

Optics EXPRESS

42. F. Hao and P. Nordlander, "Plasmonic coupling between a metallic nanosphere and a thin metallic wire," Appl. Phys. Lett. **89**(10), 103101 (2006).
43. H. Wei, F. Hao, Y. Huang, W. Wang, P. Nordlander, and H. Xu, "Polarization dependence of surface-enhanced raman scattering in gold nanoparticle- nanowire systems," Nano Lett. **8**(8), 2497–2502 (2008).
44. G. Colas des Francs, J. Grandidier, S. Massenot, A. Bouhelier, J.-C. Weeber, and A. Dereux, "Integrated plasmonic waveguides: a mode solver based on density of states formulation," Phys. Rev. B **80**(11), 115419 (2009).
45. T. Shegai, V. D. Miljkovic, K. Bao, H. Xu, P. Nordlander, P. Johansson, and M. Kall, "Unidirectional broadband light emission from supported plasmonic nanowires," Nano Lett. **11**(2), 706–711 (2011).
46. D. K. Sharma, A. Agreda, J. Barthes, G. C. Des Francs, G. P. Kumar, and A. Bouhelier, "Wave-vector analysis of plasmon-assisted distributed nonlinear photoluminescence along au nanowires," Phys. Rev. B **102**(11), 115414 (2020).
47. H. Ditlbacher, A. Hohenau, D. Wagner, U. Kreibig, M. Rogers, F. Hofer, F. R. Aussenegg, and J. R. Krenn, "Silver nanowires as surface plasmon resonators," Phys. Rev. Lett. **95**(25), 257403 (2005).
48. P. Kusar, C. Gruber, A. Hohenau, and J. R. Krenn, "Measurement and reduction of damping in plasmonic nanowires," Nano Lett. **12**(2), 661–665 (2012).
49. S. J. Al-Bader and H. A. Jamid, "Diffraction of surface plasmon modes on abruptly terminated metallic nanowires," Phys. Rev. B **76**(23), 235410 (2007).
50. D. Singh, A. Dasgupta, V. Aswathy, R. P. Tripathi, and G. P. Kumar, "Directional out-coupling of light from a plasmonic nanowire-nanoparticle junction," Opt. Lett. **40**(6), 1006–1009 (2015).
51. L. Yang, P. Li, and Z. Li, "Polarization resolved light splitting of single plasmonic nanowire emission," in *AOPC 2019: Nanophotonics*, vol. 11336 (International Society for Optics and Photonics, 2019), p. 113360C.
52. Z. Wang, H. Wei, D. Pan, and H. Xu, "Controlling the radiation direction of propagating surface plasmons on silver nanowires," Laser Photonics Rev. **8**(4), 596–601 (2014).